DOI: xxxxxxxxx
Article type: Full paper

Bifacial semi-transparent ultra-thin Cu(In,Ga)Se_2 solar cells on ITO substrate: how ITO thickness and Na doping influence the performance

Yong Li[a], Guanchao Yin[b], Martina Schmid[a]*

[a]Faculty of Physics, University of Duisburg-Essen & CENIDE, Forsthausweg 2, 47057 Duisburg, Germany

[b]School of Materials Science and Engineering, Wuhan University of Technology, Luoshi Road 122, 430070 Wuhan, China

**Corresponding author. E-mail address: yong.li@uni-due.de*

Abstract Ultra-thin Cu(In,Ga)Se_2 (CIGSe) is a promising absorber for thin-film solar cells, as it combines the advantages of low raw material consumption and high conversion efficiency. In addition, ultra-thin absorbers on transparent back contacts bring the advantage of semitransparency, which is essential for e.g. tandem or bifacial solar cells. This work optimizes ultra-thin CIGSe on In_2O_3:Sn (ITO) for application in bifacial semi-transparent ultra-thin (BSTUT) CIGSe solar cells. Firstly, 100 - 400 nm ITO were coated onto glass substrates, and it was revealed that the thickness of ITO influences its optical bandgap E_g due to the Burstein-Moss (B-M) shift. The band gap of 400 nm ITO increased by 0.14 eV compared to the 100 nm thick ITO, and the V_{oc} of the related BSTUT CIGSe solar cells raised by 0.043 V as a result of the diminished Schottky barrier Φ_b at the ITO/CIGSe interface. Secondly, 0 - 8 mg of NaF used for post deposition treatment (PDT) of the CIGSe were applied to the BSTUT solar cells. Compared to the reference without NaF, 8 mg NaF PDT enhanced the carrier density N_A from $2*10^{15}cm^{-3}$ to $1.2*10^{16}cm^{-3}$ and diminished the ITO/CIGSe Schottky barrier Φ_b by 0.21 eV. In conclusion, we found that NaF PDT can tune the carrier density of the ultra-thin CIGSe on ITO, and both thicker ITO and higher NaF PDT dose can reduce the ITO/CIGSe Schottky barrier. These discoveries enable future optimization of BSTUT CIGSe solar cells.

Key words: Bifacial, semi-transparent, ultra-thin CIGSe, ITO back contact

1. Introduction

Ultra-thin CIGSe solar cells allow to reduce the raw material consumption, compensating for the deficiency of the rare element indium [1]. They hence enable the reduction of fabrication costs and foster the increase of unit volume efficiency. By optimization of the 3-stage co-evaporation process for ultra-thin absorbers, 15.2% efficiency has been achieved on Mo substrates and the related V_{oc} (open circuit voltage) of 733 mV is comparable to the one of regular 2000 nm thick CIGSe (V_{oc} = 734 mV) [2, 3]. However, the j_{sc} (short circuit current density) of the ultra-thin devices suffered a dramatic drop (from 39.6 to 26.4 mA/cm^2) due to insufficient light absorption. To counter this, light-trapping strategies using nano-particles and back reflective mirrors have been widely explored and adopted to enhance j_{sc} [4-14]. On the other hand, the incomplete absorption of ultra-thin CIGSe can be exploited if the device is designed as bifacial semi-transparent ultra-thin solar cell (BSTUT SC) [15]. The challenge to

be overcome is the replacement of the opaque Mo by a back contact made from TCOs (transparent conductive oxides).

To find proper TCOs for BSTUT CIGSe SCs, pioneering work has been done by Nakada et al. [16-18]. By comparing AZO (ZnO:Al), FTO (SnO_2:F) and ITO (In_2O_3:Sn), Nakada found that if the CIGSe deposition temperature was kept below 500 °C for FTO and below 520 °C for ITO, the CIGSe devices can perform as well as on Mo. The photovoltaic performance will deteriorate a lot if a higher substrate temperature is used because the resistance of the TCO layer will increase dramatically [16, 17]. Kim et al. revealed that the semiconductor type of the TCO is the key issue: as CIGSe is intrinsically p-type, whilst ITO and AZO are n-type, the ITO/CIGSe/CdS/AZO structure is characterized by a double-sided bent energy band diagram [19]. Saifullah et al. tried to resolve this issue by inserting sulfurized AgGa or WO_x layers and performing NaF post-deposition treatment (PDT) [20-23]. They identified GaO_x to be formed at the ITO/CIGSe interface during the CIGSe co-evaporation, which is suspected to impede the transport of photo-generated holes [16, 24]. Furthermore, in contrast to Mo substrates which allow Na diffusion from soda-lime glass to the CIGSe absorber, ITO can block the Na diffusion and lead to poor quality of CIGSe [25]. Jan Keller et al. shows the big potential of IOH (hydrogen-doped In_2O_3), and 11% efficiency for front illumination while 6% for the rear was achieved under optimized condition, even though the hydrogen doping can be difficult to manipulate [26-28].

Given the above concerns, to achieve higher photovoltaic conversion efficiency for BSTUT SCs, attention must be paid at least in three aspects: i) The substrate temperature during the CIGSe co-evaporation must be lower than what is generally used for Mo substrates to guarantee the conductivity of the ITO is not seriously damaged. ii) The GaO_x thickness or the back-barrier height Φ_b between ITO and CIGSe must be minimized. iii) To ensure sufficient and proper Na doping for the CIGSe absorber, alkali-free glass substrates and NaF PDT doping are recommended. Recently, by optimizing the NaF PDT dose, we achieved a record efficiency of 12.9% for ultra-thin CIGSe solar cells on ITO substrate, which is mainly attributed to the carrier density N_A increase in the CIGSe bulk and the increased recombination rate at the ITO/CIGSe interface [29]. This enlightens us that the key to achieve high-efficiency BSTUT SCs is to be found in the optimization of the CIGSe layer and the ITO/CIGSe interface. Furthermore, according to the latest SCAPS simulation findings of Yin et al., the ITO/CIGSe interface - often referred to as a Schottky contact - can be improved by increasing the recombination velocity and thus facilitating the majority carrier collection [30]. To account for the precautions listed above, we take the following measures: i) The highest substrate temperature during the CIGSe co-evaporation was lowered to 450°C. ii) By optimizing the fabrication of ITO and ultra-thin CIGSe, the ITO/CIGSe interface barrier can be effectively minimized. Specifically, this paper optimizes the ITO thickness and the NaF PDT dose to modify the Schottky barrier height Φ_b at the ITO/CIGSe interface. iii) 0, 2, 4 and 8 mg NaF PDT were compared on alkali-free glass substrates.

Generally, when optimizing the overall bifacial illumination efficiency of BSTUT SCs, two aspects should be taken into account simultaneously: optical and electrical. As the rear illumination light has to penetrate the ITO and the neutral region of the CIGSe layer before reaching the space charge region (SCR), where the photo-generated carriers are separated, the optical parasitic absorption in the ITO layer and the electrical properties of the ITO should be considered thoroughly. Therefore, firstly, rear side transmission and reflection (T/R) of 100 - 400 nm ITO on glass substrate are compared theoretically and experimentally. Secondly, the influence of the optical bandgap E_g of the 100 - 400 nm thick ITO on the

photovoltaic performance is discussed. Afterwards, 0 - 8 mg NaF PDT doping doses are compared, and the contribution of chances in N_A and Φ_b on V_{oc} are estimated quantitatively.

2. Experimental section

2.1 Fabrication: Alkali-free barium boron-silicate glass (Corning 7059) was used in this study to precisely control the Na doping. All glasses underwent a standard cleaning procedure (15 minutes ultrasonic cleaning in acetone, 15 minutes in isopropanol and 15 minutes in deionized water) before being loaded into the vacuum chamber for ITO (In_2O_3:Sn) sputtering. 120 Watt DC-sputtering power and $7.5*10^{-4}$ mbar Argon atmosphere were used for the ITO fabrication. The deposition rate was 2.0 - 2.5 Å/s monitored by a calibrated quartz balance. ITO thickness variation was achieved by simply extending the sputtering time. No extra heating was applied to the substrates during the ITO growth. After transfer to a PVD (physical vapour deposition) chamber, CIGSe was co-evaporated by the standard 3-stage co-evaporation, and the substrate temperature for the first and the second stage was 410 °C and 450 °C, respectively [1, 31]. In the case of ITO thickness variation, a post-deposition treatment (PDT) with 2 mg NaF (about 3.4 nm thick) directly followed the CIGSe growth without break. The substrate temperature was kept at 360 °C during the PDT process, and 20 min were identified as optimum time to ensure all NaF was evaporated. In the other case of NaF dose variation, the samples were separated into 4 batches subject to 0, 2, 4 or 8 mg NaF PDT, respectively. For all solar cells, 60 nm CdS was coated by chemical bath deposition. Afterwards, 70 nm i-ZnO (intrinsic ZnO) and 300 nm AZO (ZnO:Al) were deposited in the same chamber by sputtering. The 10 nm Ni / 2000 nm Al finger contacts were coated by thermal evaporation before the samples were mechanically scribed into eight 1 cm $*$ 0.5 cm cells. Further fabrication details can be found in reference [29].

2.2 Characterization: The thickness of the ITO was confirmed by a Dektak step profiler from Bruker, and the sheet resistance was measured with a home-built 4-point-probe setup and found to be between 15 - 25 Ω /□ for 300 nm ITO. After the heating up during the CIGSe co-evaporation, the sheet resistance of ITO dropped to below 10 Ω /□. Transmission and reflection were measured by a Lambda 1050 UV-VIS-NIR photospectrometer. The CIGSe thickness and composition were characterized by X-ray fluorescence (XEPOS from SPECTRO along with the software XRF Analyzer Pro from AMETEK). The measured thickness is 500±10 nm for ITO thickness optimization and 491±10 nm for NaF optimization. The GGI (Ga/(Cu+Ga)) ratio) and CGI (Cu/(Cu+Ga) ratio) were found to be 0.31 and 0.85, respectively, for ITO thickness optimization and 0.32 and 0.87, respectively, for NaF optimization. The PV parameters were extracted from IV (Current-Voltage) measurements under a AAA solar simulator (WACOM) on a black cloth to exclude any reflection from the brass sample holder. Dark IV properties were measured by closing the solar simulator's shutter. Bifacial EQE (External Quantum Efficiency) was obtained from a two-source illumination system, consisting of an XBO 150W/ CR OFR model xenon lamp and a HLX 64623 GY6.35 halogen lamp. For CV (Capacitance Voltage) measurements, an LCR meter of model 895 from BK Precision is used, operating at a signal amplitude of 50 mV and a frequency of 100 kHz at room temperature. SCR (space charge region) width and doping density N_A summarized in the tables were all extracted from CV at 0 bias.

3. Results and discussion

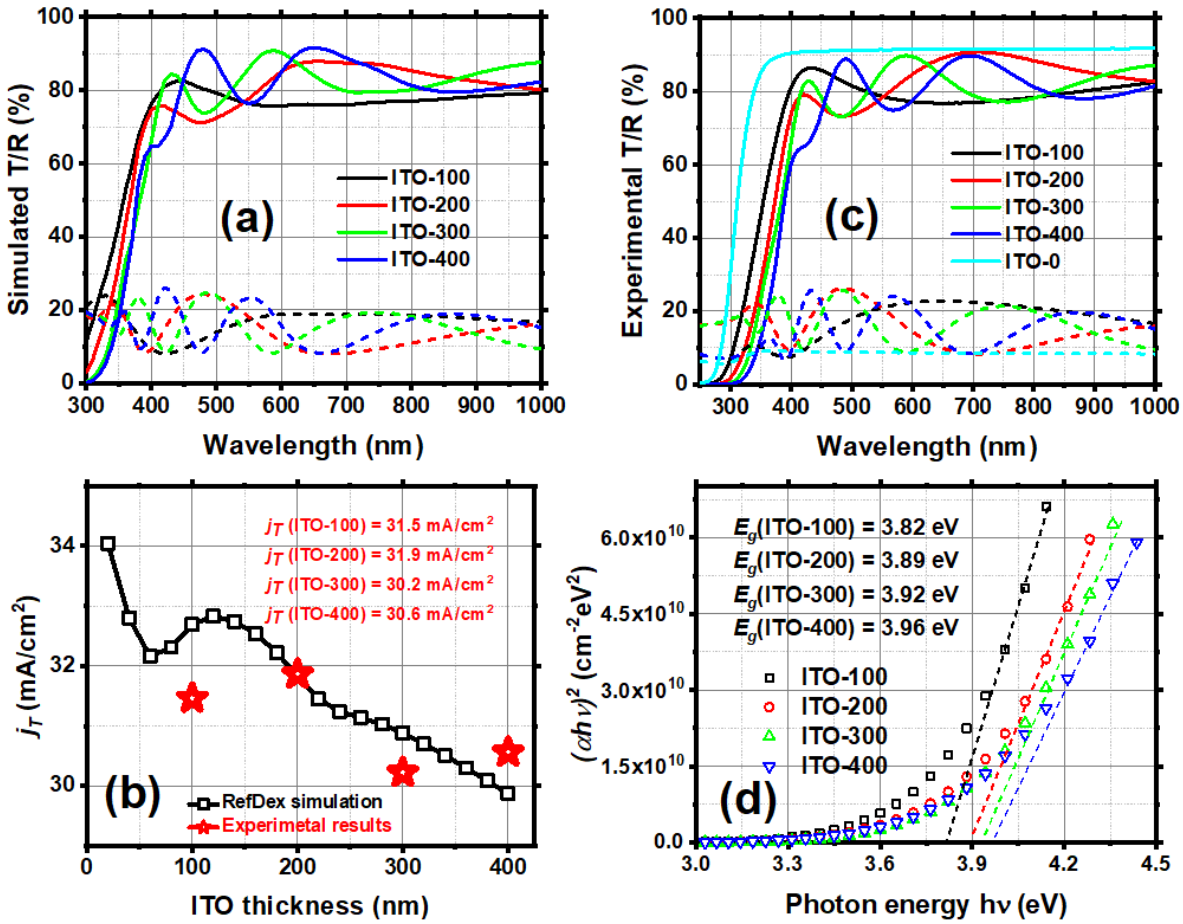

Figure 1. (a) Simulated and (c) experimentally measured transmission (solid line) and reflection (short dashed line) of glass substrate/ITO with 100, 200, 300 and 400 nm thick ITO. ITO-0 in (c) represents the bare corning glass substrate. Light illumination comes from the rear side (glass side). (b) j_T current equivalent converted from transmission by equation (1), open squares are simulated results whilst red stars relate to experimental data. (d) Derivation of the optical band gap E_g of 100 - 400 nm ITO on glass.

3.1 ITO thickness influence

The transparency of the ITO layer is critical for rear illumination efficiency as it determines the amount of light reaching the absorber layer. Presuming in a simple approach that the refractive index *n* and the extinction coefficient *k* of the ITO remain constant with thickness changes, the parasitic absorption will increase with the thickness and hence less light will reach the SCR. However, the ITO thin film gives rise to Fabry-Perot interferences, leading to the highest transmission for an optimum ITO thickness, which is different from the lowest value. Since in the solar spectrum photons of different wavelengths contain different energy, a quantitative estimation of the transmission by a current equivalent j_T is necessary:

$$j_T = \int_{350}^{1000} n(\lambda) * T(\lambda) * e * d\lambda \quad (1)$$

where $n(\lambda)$ is the number of photons of the corresponding wavelength in the solar spectrum, $T(\lambda)$ the transmission (of here the ITO/glass stack), *e* the elementary charge and λ the wavelength. **Figure 1** (a) shows *T*/*R* for ITO/glass with 100 - 400 nm ITO (ITO-100 to ITO-400) as simulated using the software RefDex [31-33]. The refractive index of ITO was extracted for an exemplary ITO layer of 200 nm deposited on glass using RefDex in reverse

calculation. ITO-100 shows one peak at 420 nm wavelength and the number of peaks for the other samples increases with the ITO thickness, which can be attributed to Fabry-Perot interferences. When the ITO thickness increment step was detailed to 20 nm (i.e., ITO-20, ITO-40, etc.), we notice that the j_T dependence on ITO thickness also shows an interference as expected (see **Figure 1** (b)). The curve reveals that j_T generally decreases with ITO thickness, yet there is a peak for an optimum ITO thickness of 120 nm.

In reality, however, the physical properties of ITO have a dependence on the film thickness, both electrically and optically. According to Kim et al., the polycrystalline size, the carrier density and the optical bandgap will increase with the ITO thickness resulting from the Burstein-Moss (B-M) shift [34]. To verify this as well as the simulation predictions, 100, 200, 300, and 400 nm ITO were coated onto glass substrates, and *T*/*R* measured from the rear side as shown in **Figure 1** (c). Experimental *T*/*R* reveal the peak at 420 nm wavelength - following the transmission drop related to the glass absorption at shorter wavelengths - and are thus in line with the RefDex simulations. Based on the experimental transmission, j_T was calculated by equation (1) and the results are marked by red stars in **Figure 1** (b). We notice an enhancement of j_T by 0.4 mA/cm^2 for ITO-200 compared to ITO-100, which is equal to the difference of 0.4 mA/cm^2 between ITO-400 and ITO-300. The biggest difference lies between 100 and 200 nm ITO on one side and 300 and 400 nm ITO on the other side. It experimentally accounts for 1.3 mA/cm^2 in average, which is close to the 2.0 mA/cm^2 difference expected from RefDex simulations. Furthermore, as shown in **Figure 1** (d), the optical band gap was deduced by the formula $(\alpha h\nu)^2 \approx h\nu - E_g$ for a direct band gap semiconductor, where $h\nu$ is the photon energy and α the absorption coefficient [35]. The latter one was extracted via $T = (1 - R)\exp(-\alpha d)$ from measured transmission *T* and reflection *R*, whereby *d* is the ITO thickness. **Figure 1** (d) shows the E_g widening from 3.82 eV to 3.96 eV as the ITO thickness increases from 100 to 400 nm. This indicates that the carrier density of the ITO is also rising according to B-M theory [34]. In general, a wider optical bandgap of a window or back contact layer (depending on the light illumination side) means less parasitic absorption and higher transmission in the short wavelength range, which is beneficial for the BSTUT SCs.

In summary, we experimentally verified that the thicker ITO layer induces a higher light loss for rear illumination (lower j_T) as the RefDex simulations predicted. On the other hand, the optical bandgap of the ITO increases with the ITO thickness as a result of the B-M shift. Compared to ITO-100, ITO-400 reveals a j_T equivalent of 1.3 mA/cm^2 higher parasitic absorption, but brought 0.14 eV gain in optical bandgap. This may explain the higher current equivalent of light loss expected from optical simulations for ITO with varying thickness but unchanged band gap. The PV (photovoltaic) performance dependence of the BSTUT CIGSe SCs on the ITO thickness will be discussed in the following part.

Table 1. Bifacial PV parameters of the BSTUT CIGSe SC on 100 - 400 nm ITO. Carrier density N_A, space charge region (*SCR*) width, and built-in electric field V_D were derived from CV measurements under dark condition. Shunt resistance R_{sh}, series resistance R_s and ideality factor *n* were extracted from dark IV curves (see **supporting information S1**). The appendix "R" (e.g. ITO-100R) means illumination from the rear side.

Sample name	ITO thickness (nm)	V_{oc} (mV)	j_{sc} (mA/cm^2)	*FF* (%)	η (%)	*SCR* width (nm)	N_A (E15 cm^{-3})	V_D (V)	R_{sh} (d*V*/d*I* @ 0 bias, Ω)	R_s (d*V*/d*I* @ V_{oc} bias, Ω)	*n*
ITO-100	100	573.1	29.5	54.9	9.3	450	5.62	0.77	498.5	6.3	1.37

ITO-200	200	609.9	28.8	55.6	9.8	408	8.53	0.95	126.9	4.9	1.52
ITO-300	300	605.8	28.7	59.0	10.3	408	7.13	0.79	214.7	3.6	1.49
ITO-400	400	621.0	28.6	60.7	10.8	397	7.35	0.77	477.2	3.9	3.20
ITO-100R	100	557.8	22.7	51.3	6.51	-	-	-	-	-	-
ITO-200R	200	579.3	22.2	49.8	6.39	-	-	-	-	-	-
ITO-300R	300	581.4	21.1	53.0	6.50	-	-	-	-	-	-
ITO-400R	400	596.2	21.4	51.8	6.63	-	-	-	-	-	-

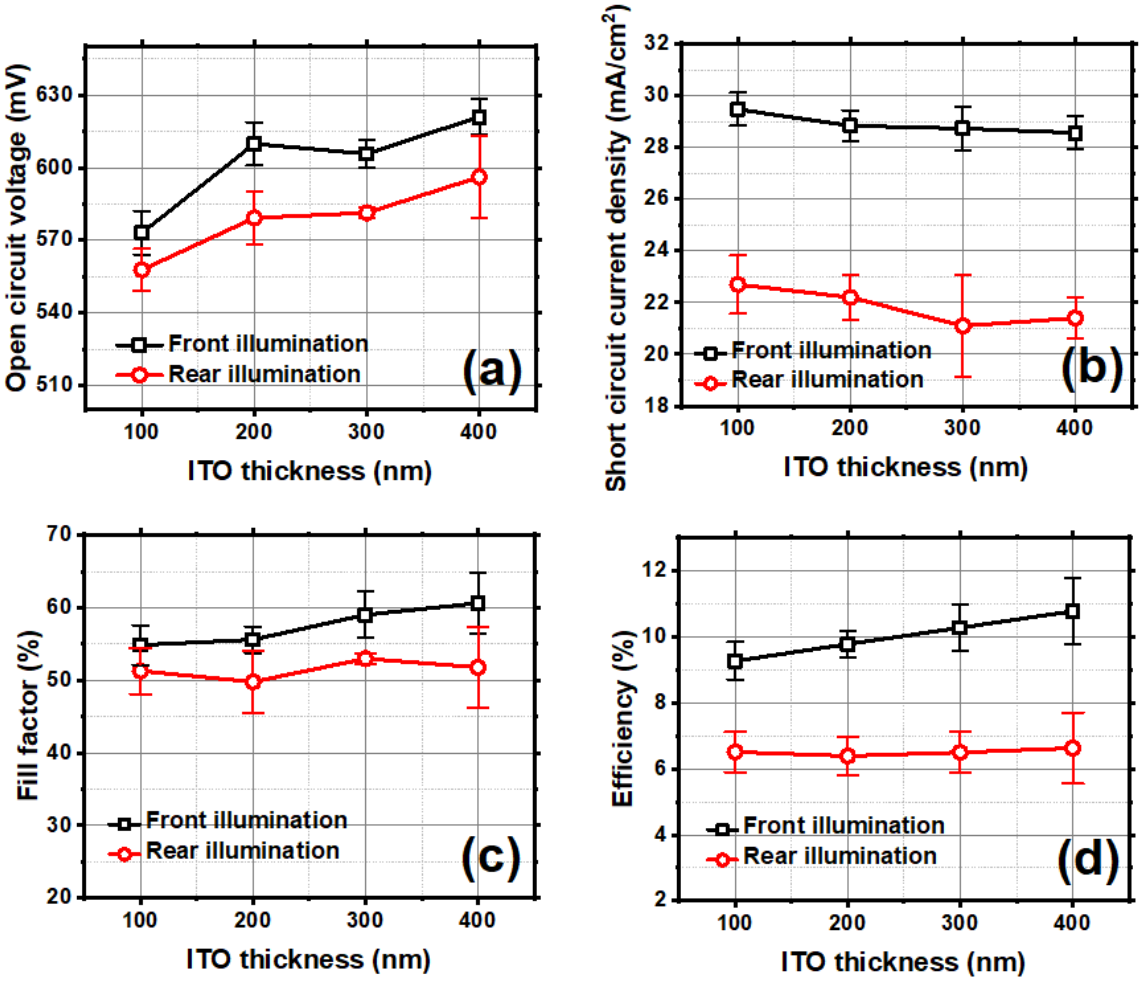

Figure 2. PV parameters (a) open circuit voltage V_{oc}, (b) short circuit current density j_{sc}, (c) fill factor *FF*, and (d) efficiency η for ITO-100, ITO-200, ITO-300 and ITO-400 in comparison. Black squares refer to front illumination and red circles to rear illumination.

Table 1 and **Figure 2** display the bifacial PV parameters depending on the ITO thickness. Most interestingly, the V_{oc} shows an increasing tendency both for front and rear illumination. To understand this, CV (capacitance voltage) characteristics are employed to extract SCR width, doping density N_A and built-in electric field V_D. For this purpose, the one-sided abrupt junction approximation $\frac{d(1/C_D^2)}{dV} = -\frac{2}{q\varepsilon_s N_A}$ (C_D is the depletion region capacitance, ε_s the

dielectric constant of CIGSe and q the elementary charge) [36, 37] is used for the CdS/CIGSe interface and the results are listed in **Table 1**. The SCR width shrinks continuously from 450 to 397 nm when increasing the ITO thickness from 100 to 400 nm. N_A and V_D, however, just jump in the range from 5.6 - 8.5*10^{15}cm^{-3} and 0.77 - 0.95 V, respectively. We did not see a clear consistent trend between V_D, N_A and V_{oc} (a higher N_A and V_D would be expected to lead to a higher V_{oc} [29]) as we do in the following part of investigating NaF PDT. This implies that the V_{oc} change was not primarily determined by the CdS/CIGSe main junction, which is the one the CV properties are relating to, but by the ITO layer or/and the ITO/CIGSe interface.

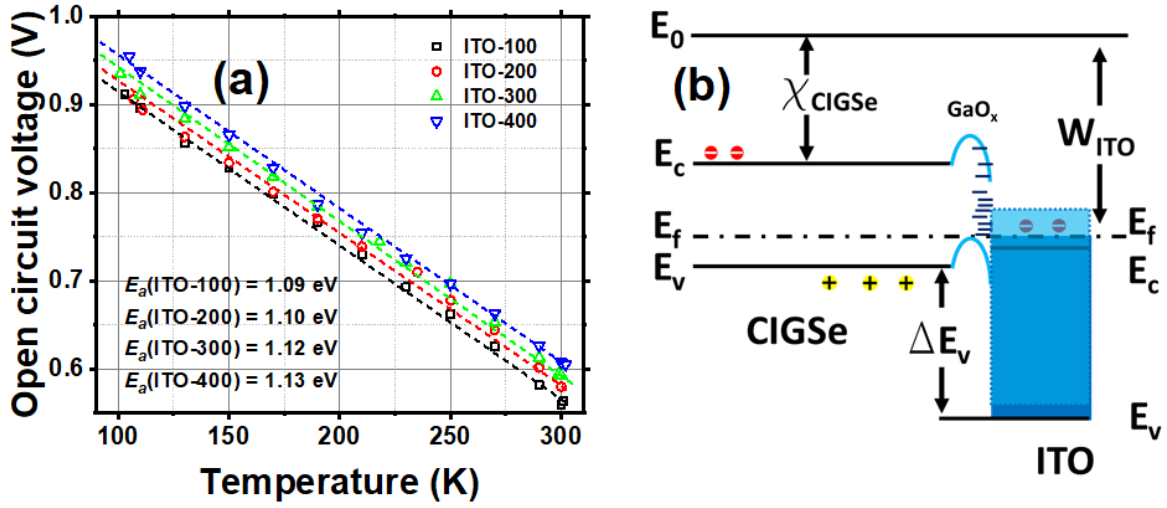

Figure 3. (a) Temperature dependent open circuit voltage of ITO-100 to ITO-400 and derived activation energy E_a, (b) schematic band diagram of the CIGSe/ITO back contact.

To quantitatively estimate the back barrier Φ_b at the ITO/CIGSe interface, IVT (temperature-dependent IV) measurements under front illumination were used to extract the activation energy E_a for the four ITO thicknesses as shown in **Figure 3**. The activation energy relates to the back barrier via [12, 38]

$$E_a = E_g - \Phi_b \qquad (2)$$

where E_g is the CIGSe bandgap. As it increases from 1.09 eV to 1.13 eV, while E_g remains at 1.14 eV according to the EQE (external quantum efficiency, see **supporting information S2**), we deduce that Φ_b reduces from 0.05 to 0.01 eV. This can contribute 40 mV gain in V_{oc}, which is consistent with the V_{oc} increase of 48 mV for cells on ITO-400 compared to those on ITO-100.

Now that the V_{oc} gain was clearly linked to the diminished Φ_b from the device perspective, the remaining question is the origin of the barrier change from the material point of view. To better illustrate the two possible mechanisms, **Figure 3** (b) shows the bandgap mismatch at the ITO/CIGSe interface. ΔE_v marks the valance band offset between ITO and CIGSe. The dark blue coloured box corresponds to ITO-100 while the light blue one with dotted line border represents ITO-400. $E_g(CIGSe)$ remains unchanged whereas $E_g(ITO)$ widened from 3.82 to 3.96 eV due to the B-M shift [39, 40]. The first possibility for the reduction of Φ_b is a lower valance band offset ΔE_v between CIGSe and ITO for the thicker ITO. As **Figure 3** (b) shows, $\Delta E_v = W_{ITO} + E_g(ITO) - \chi_{CIGSe} - E_g(CIGSe)$ [41], with W_{ITO} the work function of ITO and χ_{CIGSe} the CIGSe electron affinity. Considering that a thicker ITO induces a wider

$E_g(ITO)$ but lower W_{ITO}, and the W_{ITO} decrement is bigger than the $E_g(ITO)$ increment according to Yasushi Sato et al. [42], the overall ΔE_v will be diminished. This also explains that the $E_g(ITO)$ increment is 0.14 eV while the Φ_b decrement is only 0.04 eV, as Φ_b is influenced by ΔE_v instead of $E_g(ITO)$ directly. The second possibility is that the properties like thickness and defect density of the interfacial GaO_x are influenced by the ITO layer thickness. As XRD measurements show (**supporting information S3**), the thicker ITO has a preferential orientation in the (222) direction which may influence the GaO_x formation, which is decided by the ITO morphology [34]. Besides, ITO with a smaller work function (originating from a larger E_g) was found beneficial in organic solar cells for hole transport/collection and in light emitting devices as anode contact due to higher carrier density and wider bandgap [34, 35, 43].

The short-circuit current density j_{sc} was decreasing under front illumination with increasing ITO thickness. Parasitic absorption from ITO can be considered negligible since the light is passing the absorber first. This is underlined by comparing the optical j_T loss calculated for the entire device, which is only 0.15 - 0.23 mA/cm^2 compared to the j_{sc} decrease of 0.7 - 0.9 mA/cm^2. Therefore, the j_{sc} loss is mostly caused by the electrical loss of recombination. Generally, the diffusion length of the minority carriers is decided by the interface as well as by the bulk lifetime. The majority carriers in the SCR region are depleted, and the photo-generated carriers go through the SCR mainly by drifting, thus the recombination happening in the SCR is low and the diffusion length is long. The wider the SCR is, the longer the bulk lifetime will be [37]. Since the diminished Φ_b shortens the interface lifetime and the narrower SCR shortens the bulk lifetime of the carriers, the diffusion length will reduce for cells with thicker ITO. Consequently, recombination increases and j_{sc} diminishes.

As for the *FF* increase shown in **Figure 2**, we can estimate the V_{oc}-originated contribution by the equation [44]

$$FF_0 = \frac{v_{oc} - \ln(v_{oc}+0.72)}{v_{oc}+1} \quad (3)$$

where $v_{oc} = \frac{q}{nkT} V_{oc}$ is the normalized open circuit voltage. If the diode factor n takes an average value of 1.5, then the V_{oc} improvement from 573 to 621 mV (ITO-100 to ITO-400) will lead to a FF_0 enhancement of 1.3% absolute. This part originating from the diminished Φ_b is smaller than the observed *FF* increment of 5.8%. As *FF* is essentially influenced by R_s and R_{sh}, we use the following expression to estimate the impact of the modified resistance values [44]:

$$FF = FF_0 \left\{(1 - 1.1 r_s) + \frac{r_s^2}{5.4}\right\} \left\{1 - \frac{v_{oc}+0.7}{v_{oc}} \frac{FF_0}{r_{sh}} [(1 - 1.1 r_s) + \frac{r_s^2}{5.4}]\right\} \quad (4)$$

FF_0 means the fill factor without shunt and series resistance, r_s and r_{sh} mean normalized series resistance and shunt resistance respectively, for details see reference [44]. Comparing ITO-400 to ITO-100 R_s dropped from 6.3 to 3.9 Ω while R_{sh} decreases from 498.5 to 477.2 Ω (see **Table 1**). According to formula (4) the *FF* can be levelled up by 8% which is closer to the experimental *FF* gain of 5.8% [44]. This calculated change in *FF* may also include the above contribution of the decreased barrier, which can be correlated to a decreased R_s.

Finally, concerning the rear illumination PV performance, as shown in **Figure 2** (a) and (b), V_{oc} and j_{sc} are behaving similarly as for front illumination. The trend in V_{oc}, on the one hand, is understandable in the same way as discussed for front illumination, i.e. it is caused by the diminished Φ_b at the ITO/CIGSe interface. On the other hand, the reduction in j_{sc} for rear

illumination can essentially be attributed to ITO parasitic absorption: compared to ITO-100, the j_{sc} loss observed experimentally for ITO-400 is 1.3 mA/cm^2, which almost equals the j_T difference calculated from *T*/*R* measurements of 400 and 100 nm thick ITO. Interestingly, j_{sc} of ITO-300 is 0.3 mA/cm^2 lower than ITO-400, close to the 0.4 mA/cm^2 difference in j_T, which again tells us the decisive importance of the ITO/glass transmission under rear illumination. The *FF*, however, shows a fluctuating change under rear illumination. When the illumination comes from the rear side, the density of photo-generated carriers is higher at the back side of the device. As the neutral region is wider for thicker ITO, the collection efficiency will be lower in this case. In the end, the changes in the V_{oc} and j_{sc} level out and the efficiency is in the range of 6.39-6.63% with a small variation.

3.2 NaF PDT doping influence

Table 2. Bifacial PV parameters of the BSTUT CIGSe SC with 0 - 8 mg NaF PDT doping. Carrier density N_A, space charge region (SCR) width at 0-volt bias, and built-in electric field V_D were derived from CV measurements under dark condition. Shunt resistance R_{sh} and series resistance R_s were derived from IV measurements under dark condition (see **supporting information S5**). The appendix "R" (e.g. NaF_0R) relates to measurements under rear illumination.

Sample name	NaF PDT dose (mg)	V_{oc} (mV)	j_{sc} (mA/cm^2)	*FF* (%)	η (%)	N_A (E15 cm^{-3})	SCR width (nm)	V_D(V)	R_{sh} (d*V*/d*I* @ 0 bias, Ω)	R_s (d*V*/d*I* @ V_{oc} bias, Ω)
NaF_0	0	517.3	29.2	57.3	8.7	2.19	588	0.53	1174.5	10.8
NaF_2	2	610.0	27.6	67.1	11.3	6.91	380	0.69	2972.8	5.9
NaF_4	4	621.2	28.2	67.1	11.8	7.95	369	0.72	328.6	5.7
NaF_8	8	630.4	28.2	62.8	11.2	11.63	318	0.75	410.9	4.4
NaF_0R	0	474.0	19.0	47.5	4.3	-	-	-	-	-
NaF_2R	2	581.7	19.1	57.0	6.3	-	-	-	-	-
NaF_4R	4	585.4	17.3	62.9	6.4	-	-	-	-	-
NaF_8R	8	597.2	16.3	58.2	5.7	-				

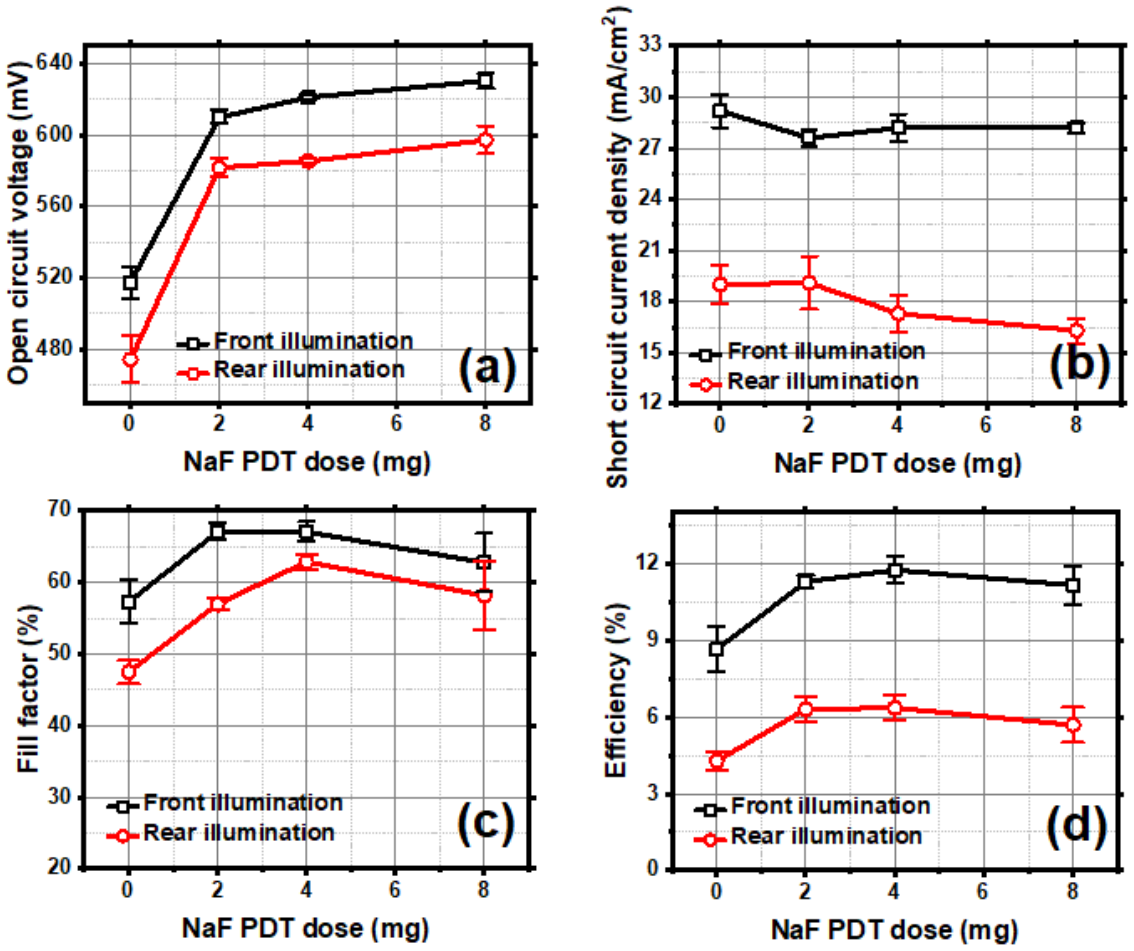

Figure 4. PV parameters (a) open circuit voltage V_{oc}, (b) short circuit current density j_{sc}, (c) fill factor *FF*, and (d) efficiency η for the samples with 0, 2, 4, or 8 mg NaF PDT (NaF_0, NaF_2, NaF_4 and NaF_8) in comparison. Black squares refer to front illumination and red circles to rear illumination.

Na doping has always played an important role in controlling the CIGSe quality, although there is a remaining discussion about the mechanism how it influences the CIGSe grain boundaries [45, 46]. Our previous study has shown that NaF doping by post deposition treatment (PDT) can modify the carrier density N_A in the CIGSe bulk as well as the recombination rate at the ITO/CIGSe interface [29]. The current contribution focuses on the quantitative correlation between bifacial PV performance and Na doping dose. Whereas for the experiments on various thicknesses of ITO back contact, NaF PDT was performed directly after the 3-stage co-evaporation, for the variation of NaF dose one batch of CIGSe absorbers was taken out of the PVD (physical vapour deposition) chamber and divided into four groups. The samples of each group were then separately put back into the PVD chamber along with 0, 2, 4 and 8 mg NaF powder, respectively, and subject to the PDT process. The corresponding samples are referred to as NaF_0, NaF_2, NaF_4 and NaF_8. In this way, the differences in composition (in particular Cu and Ga ratio) as well as in CIGSe thickness between the samples were minimized. The ITO thickness used is 300 nm, as ITO-300 showed adequate high efficiency under both front and rear illumination, and the overall thickness of the BSTUT solar cells should be as thin as possible to ensure its transparency.

Table 2 summarizes the bifacial PV parameters of the BSTUT CIGSe SCs with 0 - 8 mg NaF PDT, along with the carrier density N_A, space charge region width, built-in electric field V_D, shunt resistance R_{sh}, and series resistance R_s. **Figure 4** visualizes the trends of the bifacial PV parameters. Firstly, V_{oc} shows a tremendous gain of approx. 100 mV as the NaF PDT dose increases. As the NaF doping mainly modifies the N_A and the recombination velocity (as a result of diminished Φ_b) at the ITO/CIGSe interface [26], here we focus on quantifying the contribution of those two factors [29]. For investigating the influence of the acceptor doping density N_A we employ the formula [47]:

$$V_{oc} = \frac{kT}{q} ln[\frac{(N_A+\Delta n)\Delta n}{n_i^2}] \quad (5)$$

where Δn is the excess carrier concentration, n_i the intrinsic carrier concentration and kT/q the thermal voltage. By setting Δn = 1*10^{14}cm^{-3} and n_i = 8.6*10^9 cm^{-3} we can approach the range of experimental V_{oc} results and vary N_A in the range from 2 - 12*10^{15} cm^{-3} as derived from CV measurements. According to formula (5), V_{oc} then varies in the range from 559 - 604 mV, i.e. is 45 mV higher for NaF_8 than for NaF_0. This is about half of the V_{oc} change measured for NaF_0 compared NaF_8, which is 630 vs 517 mV, i.e. 113 mV difference. Consequently, the N_A modification in the CIGSe bulk is only partially responsible for the V_{oc} gain, while the remaining V_{oc} gain may originate from the reduction of the back barrier Φ_b. Considering formula (2) again as well as that the CIGSe bandgap E_g remains unchanged for all NaF doses (estimated from the EQE in **Figure 5**) we find the following from IVT data fitting (**supporting information S4**): compared to NaF_0, E_a of NaF_2 is 130 meV higher, which is close to the observed V_{oc} gain of 92.7 mV. Compared to NaF_2, E_a of NaF_4 and NaF_8 shows a continuous increase by firstly 20 and then another 60 meV. This expected V_{oc} gain now is even larger than the measured gain of 11 and 9 mV, respectively, which may be linked to the V_{oc} deficit [48-50]. It is worth to point out that the IVT estimated E_a increase should include the N_A boost in the CIGSe bulk along with the Φ_b diminishment at the ITO/CIGSe interface, because the V_{oc}-T is extracted from the whole device. Therefore, the diminished Φ_b partially contributes the V_{oc} gain in addition to the N_A enhancement [29].

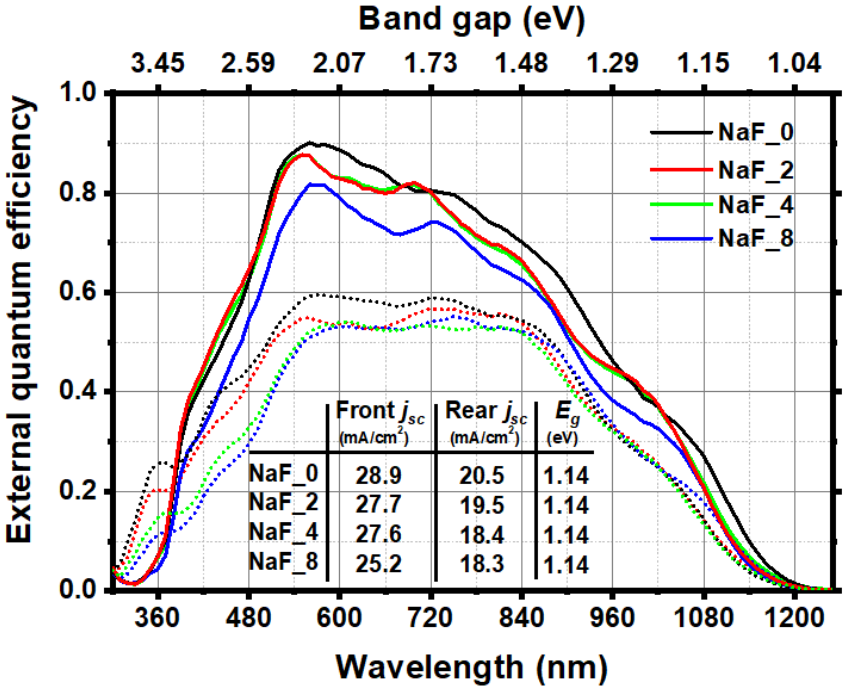

Figure 5. Bifacial EQE of the samples NaF_0, NaF_2, NaF_4 and NaF_8. The solid line refers to front illumination and the dotted line to the rear illumination, respectively. The inserted table summarizes the EQE integrated current density j_{sc} and the CIGSe bandgap E_g obtained from the derivative.

Secondly, we observe from **Figure 4** a decreasing curve for j_{sc} with increasing Na content. Commonly, the anomaly of increased V_{oc} but reduced j_{sc} is attributed to the high recombination of photo-generated minority carriers at the interfaces [41]. Generally, recombination at the interfaces of incident light direction affects more the short-wavelength in the EQE response, and a low L_p rather keeps the EQE shape but lowers its overall level [27, 51]. In our case, the Na concentration is higher at the ITO/CIGSe side than at the CdS/CIGSe side, as shown by GD-OES in our previous work reference [29]. This implies that the congregation of Na at the ITO/CIGSe interface can induce higher recombination velocity hence reduce the j_{sc} [29]. Meanwhile, the increase of N_A from $2*10^{15}$ cm^{-3} to $1.2*10^{16}$ cm^{-3} will proportionally shorten L_p and thus further aggravate the recombination loss in the CIGSe bulk [41].

To further identify the j_{sc} decrease, bifacial EQE was measured and is shown in **Figure 5**. The j_{sc} integrated from the EQE shows a decreasing trend consistent with the IV results. For front illumination, the EQE data for NaF_0, NaF_2 and NaF_4 are overlapping in the wavelength range from 300 - 540 nm, which means that the front interface recombination loss in NaF_2 and NaF_4 is comparable to the one of NaF_0 here. However, in the range from 540 - 1200 nm, the EQE of NaF_2 and NaF_4 shows a lower percentage than NaF_0 (with an exception at around 700 nm). This observation can be interpreted as shorter average diffusion length L_p for NaF_2 and NaF_4 than NaF_0 and be linked to the increased N_A. NaF_8 shows an even more severe decrease over the whole wavelength range, which can be linked to the highest recombination in the CIGSe bulk.

When it comes to the rear illumination EQE, we notice that there is an overall increase in the short wavelength range compared to the front EQE, and a conspicuous peak at 360 nm for all NaF doses. Judging by the corresponding bandgap, the overall increase stems from the absence of CdS parasitic absorption, and the peak is attributed to interference between the thin film layers. In the wavelength range from 300 - 540 nm, there is a significant drop in EQE with increasing Na doping, which may be linked to an increasing recombination velocity at the ITO/CIGSe interface as the Na concentration increases. In the case of rear illumination, the density of photo-generated carriers is high close to the ITO/CIGSe interface, which can intensify their annihilation at this position. The wavelength ranges from 540 - 840 nm is characterized by a plateau, which may be interpreted as a combination of two effects: In case of rear illumination, longer wavelength light generally may be absorbed closer to the SCR due to its higher penetration depth. On the other hand, for ultra-thin solar cells, long wavelength light is subject to transmission and hence a related reduction in EQE as also visible for the case of front illumination. Interestingly, the EQE above 700 nm is hardly suffering from a reduction with increasing Na doping, which indicates a stronger effect of Na on the rear interface.

Coming to the *FF*, according to formula (3), a V_{oc} increase from 517 to 610 mV (NaF_0 to NaF_2) results in a FF_0 increment of 2.7%, which is smaller than the experimentally measured difference of 9.8%. This implies that the series resistance drop from 10.8 to 5.9 Ω also contributes to the *FF* gain for NaF_2, which according to formula (4) accounts for 18%. When the V_{oc} continues to increase from 610 to 621 mV (for NaF_4), the FF_0 increase according to formula (3) is only 0.3%, whereas formula (4) considering R_s and R_{sh} gives 0.6% decrease. Thus, overall the *FF* of NaF_4's would be expected to decrease by 0.3%, which is

comparable to the stagnating measured value of 67.1%. For NaF_8 the trend of experimental *FF* reduction continues despite an increased V_{oc}, which may be caused by higher recombination in the device.

Overall, the efficiency follows the trend of *FF*. Interestingly, the rear illumination efficiency shows a parallel trend with the front illumination in **Figure 4** (d), which means under rear illumination the light loss in the ITO/glass layers is almost the same for all NaF doses. The highest efficiency is reached for NaF_4 with 11.8% under front and 6.4% under rear illumination. Compared to the record efficiency of 15.2% for ultra-thin CIGSe on Mo, there is still room for improvement. Further optimization of alkali doping can play a role mostly with respect to V_{oc} and *FF*, whilst concepts for light management like mirrors and nanoparticles are required to boost j_{sc} [2, 8, 12]. Overall, it may not be forgotten that losses in performance of BSTUT CIGSe solar cells appearing on the first glance, are in parts the key for their application in concepts where semitransparency is required.

4. Conclusion

In summary, this contribution investigated bifacial semi-transparent ultra-thin (BSTUT) CIGSe solar cells under the aspects of ITO back contact thickness and Na doping. In the first part of ITO thickness optimization, we discovered that a thicker ITO comes with a widened optical bandgap due to the B-M shift, leading to an enhanced V_{oc} (573 to 621 mV) via a back barrier reduction under front illumination. Yet the front j_{sc} is reduced by 0.9 mA/cm^2 mainly due to the increasing recombination. Compared to ITO-100R, the rear illumination j_{sc} of ITO-400R decreased by 1.3 mA/cm^2, which could be directly linked to the optical loss of ITO parasitic absorption. Yet, the V_{oc} improved by 38 mV due to the diminished Schottky barrier Φ_b at the ITO/CIGSe interface, which levelled the final rear efficiency at 6.6%. Secondly, it was revealed that 0 - 8 mg NaF PDT can modify the acceptor carrier density N_A of CIGSe from 2*10^{15} to 12*10^{15} cm^{-3}. However, the N_A enhancement can only partly explain the front V_{oc} increase from 517 to 630 mV, which implies the NaF PDT also diminishes the Φ_b at the ITO/CIGSe interface. Meanwhile, j_{sc} reveals a decreasing trend as a result of increasing recombination. For the rear illumination, the PV parameters of different NaF PDT doses show a parallel trend to those of front illumination. With overall NaF PDT optimization, 11.8% efficiency under front and 6.4% under rear illumination were achieved. In the future, light management methods will play an important role to either enhance j_{sc} or to enable an efficient coupling of non-absorbed light for other exploitation. In this way, BSTUT CIGSe SCs can play an important role for applications in e.g. photovoltaic roofs, agrivoltaics, solar trees or solar window glasses.

Acknowledgement

All authors would like to express their sincere gratitude to Tristan Köhler and Klaus Pärschke for technical support, Jan Lucaßen, Sedaghat Setareh and Yao Gao for discussions. Alexander Poßberg, Bauelemente der Höchstfrequenzelektronik (BHE, University of Duisburg-Essen) is acknowledged for support with XRD characterization. The XRF and GD-OES measurements were performed on an instrument funded by the Deutsche Forschungsgemeinschaft (DFG, German Research Foundation) – INST 20876/324-1 FUGG and are acknowledged as follows: “Gefördert durch die Deutsche Forschungsgemeinschaft (DFG) – Projektnummer INST 20876/324-1 FUGG”. Yong Li receives the subsidy from the Chinese Scholarship Committee, and Guanchao Yin the funding from the National Natural Science Foundation of China (NSFC, 51802240).

References

[1] G. Yin, V. Brackmann, V. Hoffmann, M. Schmid, Enhanced performance of ultra-thin Cu(In,Ga)Se2 solar cells deposited at low process temperature, Sol. Energy Mater. Sol. Cells, 132 (2015) 142-147.

[2] L.M. Mansfield, A. Kanevce, S.P. Harvey, K. Bowers, C. Beall, S. Glynn, I.L. Repins, Efficiency increased to 15.2% for ultra-thin Cu(In,Ga)Se2 solar cells, Prog. Photovoltaics Res. Appl., (2018) 1-6.

[3] M. Nakamura, K. Yamaguchi, Y. Kimoto, Y. Yasaki, T. Kato, H. Sugimoto, Cd-Free Cu(In,Ga)(Se,S)2 Thin-Film Solar Cell With Record Efficiency of 23.35%, IEEE J. Photovoltaics, 9 (2019) 1863-1867.

[4] L. Gouillart, A. Cattoni, J. Goffard, F. Donsanti, G. Patriarche, M. Jubault, N. Naghavi, S. Collin, Development of reflective back contacts for high-efficiency ultrathin Cu(In,Ga)Se2 solar cells, Thin Solid Films, 672 (2019) 1-6.

[5] L. Gouillart, S. Collin, W.-C. Chen, A. Cattoni, J. Goffard, L. Riekehr, J. Keller, M. Jubault, N. Naghavi, M. Edoff, Reflective Back Contacts for Ultrathin Cu(In,Ga)Se2-Based Solar Cells, IEEE J. Photovoltaics, 10 (2020) 250-254.

[6] C.v. Lare, G. Yin, A. Polman, M. Schmid, light coupling and trapping in ultrathin Cu(In,Ga)Se2 solar cells using dielectric scattering patterns, ACS Nano, 9 (2015) 9603-9613.

[7] M. Schmid, P. Manley, A. Ott, M. Song, G. Yin, Nanoparticles for light management in ultrathin chalcopyrite solar cells, Journal of Materials Research, 31 (2016) 3273-3289.

[8] M. Schmid, Review on light management by nanostructures in chalcopyrite solar cells, Semiconductor Science and Technology, 32 (2017) 043003.

[9] G. Yin, A. Steigert, P. Andrae, M. Goebelt, M. Latzel, P. Manley, I. Lauermann, S. Christiansen, M. Schmid, Integration of plasmonic Ag nanoparticles as a back reflector in ultra-thin Cu(In,Ga)Se2 solar cells, Applied Surface Science, 355 (2015) 800-804.

[10] G. Yin, P. Manley, M. Schmid, Light absorption enhancement for ultra-thin Cu(In1−xGax)Se2 solar cells using closely packed 2-D SiO2 nanosphere arrays, Sol. Energy Mater. Sol. Cells, 153 (2016) 124-130.

[11] G. Yin, M. Song, S. Duan, P. Manley, D. Greiner, C.A. Kaufmann, M. Schmid, Well-Controlled Dielectric Nanomeshes by Colloidal Nanosphere Lithography for Optoelectronic Enhancement of Ultrathin Cu(In,Ga)Se2 Solar Cells, ACS Appl Mater Interfaces, 8 (2016) 31646-31652.

[12] G. Yin, M.W. Knight, M.-C. van Lare, M.M. Solà Garcia, A. Polman, M. Schmid, Optoelectronic Enhancement of Ultrathin CuIn1-xGaxSe2Solar Cells by Nanophotonic Contacts, Adv. Opt. Mater., 5 (2017) 1600637.

[13] G. Yin, P. Manley, M. Schmid, Light trapping in ultrathin CuIn1-xGaxSe2 solar cells by dielectric nanoparticles, Sol. Energy, 163 (2018) 443-452.

[14] G. Yin, M. Song, M. Schmid, Rear point contact structures for performance enhancement of semi-transparent ultrathin Cu(In,Ga)Se2 solar cells, Sol. Energy Mater. Sol. Cells, 195 (2019) 318-322.

[15] D. Kim, S.S. Shin, S.M. Lee, J.S. Cho, J.H. Yun, H.S. Lee, J.H. Park, Flexible and Semi‐Transparent Ultra‐Thin CIGSe Solar Cells Prepared on Ultra‐Thin Glass Substrate: A Key to Flexible Bifacial Photovoltaic Applications, Adv. Funct. Mater., (2020) 2001775.

[16] T. Nakada, Microstructural and diffusion properties of CIGS thin film solar cells fabricated using transparent conducting oxide back contacts, Thin Solid Films, 480-481 (2005) 419-425.

[17] T. Nakada, Y. Hirabayashi, T. Tokado, D. Ohmori, T. Mise, Novel device structure for Cu(In,Ga)Se2 thin film solar cells using transparent conducting oxide back and front contacts, Sol. Energy, 77 (2004) 739-747.

[18] T. Nakada, S. Shirakata, Impacts of pulsed-laser assisted deposition on CIGS thin films and solar cells, Sol. Energy Mater. Sol. Cells, 95 (2011) 1463-1470.

[19] K. Kim, W.N. Shafarman, Alternative device structures for CIGS-based solar cells with semi-transparent absorbers, Nano Energy, 30 (2016) 488-493.

[20] M. Saifullah, S. Ahn, J. Gwak, S. Ahn, K. Kim, J. Cho, J.H. Park, Y.J. Eo, A. Cho, J.-S. Yoo, J.H. Yun, Development of semitransparent CIGS thin-film solar cells modified with a sulfurized-AgGa layer for building applications, J. Mater. Chem. A, 4 (2016) 10542-10551.

[21] M. Saifullah, K. Kim, R. Shahzad, J. Gwak, J.-S. Cho, J.-S. Yoo, J.H. Yun, J.H. Park, Insertion of the AGS layer at the CIGSe/ITO interface: A way to reduce the formation of the GaO x interfacial phase in CIGSe solar cells, Sol. Energy Mater. Sol. Cells, 178 (2018) 29-37.

[22] M. Saifullah, S. Rasool, S. Ahn, K. Kim, J.S. Cho, J.S. Yoo, W.S. Shin, J.H. Yun, J.H. Park, Performance and Uniformity Improvement in Ultrathin Cu(In,Ga)Se2 Solar Cells with a WOx Nano-Interlayer at the Absorber/Transparent Back-Contact Interface, ACS Applied Materials and Interfaces, (2019) 655-665.

[23] M. Saifullah, D. Kim, J.-S. Cho, S. Ahn, S. Ahn, J.H. Yun, H.S. Lee, J.H. Park, The role of NaF post-deposition treatment on the photovoltaic characteristics of semitransparent ultrathin Cu(In,Ga)Se2 solar cells prepared on indium-tin-oxide back contacts: a comparative study, J. Mater. Chem. A, 7 (2019) 21843-21853.

[24] M.D. Heinemann, V. Efimova, R. Klenk, B. Hoepfner, M. Wollgarten, T. Unold, H.-W. Schock, C.A. Kaufmann, Cu(In,Ga)Se2 superstrate solar cells: prospects and limitations, Prog. Photovoltaics Res. Appl., 23 (2015) 1228-1237.

[25] Y.-S. Son, H. Yu, J.-K. Park, W.M. Kim, S.-Y. Ahn, W. Choi, D. Kim, J.-h. Jeong, Control of Structural and Electrical Properties of Indium Tin Oxide (ITO)/Cu(In,Ga)Se2

Interface for Transparent Back-Contact Applications, J. Phys. Chem. C, 123 (2019) 1635-1644.

[26] J. Keller, F. Chalvet, J. Joel, A. Aijaz, T. Kubart, L. Riekehr, M. Edoff, L. Stolt, T. Törndahl, Effect of KF absorber treatment on the functionality of different transparent conductive oxide layers in CIGSe solar cells, Prog. Photovoltaics Res. Appl., 26 (2018) 13-23.

[27] J. Keller, W.-C. Chen, L. Riekehr, T. Kubart, T. Törndahl, M. Edoff, Bifacial Cu(In,Ga)Se2 solar cells using hydrogen-doped In2O3 films as a transparent back contact, Prog. Photovoltaics Res. Appl., (2018).

[28] J. Keller, N. Shariati Nilsson, A. Aijaz, L. Riekehr, T. Kubart, M. Edoff, T. Törndahl, Using hydrogen-doped In2O3 films as a transparent back contact in (Ag,Cu)(In,Ga)Se2 solar cells, Prog. Photovoltaics Res. Appl., 26 (2018) 159-170.

[29] Y. Li, G. Yin, Y. Gao, T. Köhler, J. Lucaßen, M. Schmid, Sodium control in Ultrathin Cu(In,Ga)Se2 solar cells on transparent back contact for efficiencies beyond 12%, Sol. Energy Mater. Sol. Cells, 223 (2021).

[30] Y. Tu, Y. Li, R. Klenk, G. Yin, M. Schmid, Is a passivated back contact always beneficial for Cu(In,Ga)Se2 solar cells, in: Prog. Photovoltaics Res. Appl., Submitted, 2021.

[31] G. Yin, P. Manley, M. Schmid, Influence of substrate and its temperature on the optical constants of CuIn1−xGaxSe2thin films, Journal of Physics D: Applied Physics, 47 (2014) 135101.

[32] P. Manley, G. Yin, M. Schmid, A method for calculating the complex refractive index of inhomogeneous thin films, Journal of Physics D: Applied Physics, 47 (2014).

[33] G. Yin, C. Merschjann, M. Schmid, The effect of surface roughness on the determination of optical constants of CuInSe2 and CuGaSe2 thin films, J. Appl. Phys., 113 (2013) 213510.

[34] H. Kim, J.S. Horwitz, G. Kushto, A. Piqué, Z.H. Kafafi, C.M. Gilmore, D.B. Chrisey, Effect of film thickness on the properties of indium tin oxide thin films, J. Appl. Phys., 88 (2000) 6021-6025.

[35] H. Kim, C.M. Gilmore, A. Piqué, J.S. Horwitz, H. Mattoussi, H. Murata, Z.H. Kafafi, D.B. Chrisey, Electrical, optical, and structural properties of indium–tin–oxide thin films for organic light-emitting devices, J. Appl. Phys., 86 (1999) 6451-6461.

[36] L.C. Kimerling, Influence of deep traps on the measurement of free-carrier distributions in semiconductors by junction capacitance techniques, J. Appl. Phys., 45 (1974) 1839-1845.

[37] S.M. Sze, K.K. Ng, Physics of semiconductor devices, John Wiley & Sons, Hoboken, New Jersey. Published simutaneously in Canada., 2007.

[38] S.S. Hegedus, W.N. Shafarman, Thin-film solar cells: device measurements and analysis, Prog. Photovoltaics Res. Appl., 12 (2004) 155-176.

[39] P. Prepelita, M. Filipescu, I. Stavarache, F. Garoi, D. Craciun, Transparent thin films of indium tin oxide: Morphology–optical investigations, inter dependence analyzes, Applied Surface Science, 424 (2017) 368-373.

[40] J.-H. Kim, T.-Y. Seong, K.-J. Ahn, K.-B. Chung, H.-J. Seok, H.-J. Seo, H.-K. Kim, The effects of film thickness on the electrical, optical, and structural properties of cylindrical, rotating, magnetron-sputtered ITO films, Applied Surface Science, 440 (2018) 1211-1218.

[41] R. Scheer, H.-W. Schock, Chalcogenide Photovoltaics Physics, Technologies, and Thin Film Devices, WILEY-VCH Verlag & Co. KGaA, Boschstr. 12, 69469 Weinheim, Germany, 2011.

[42] Y. Sato, T. Ashida, N. Oka, Y. Shigesato, Carrier Density Dependence of Optical Band Gap and Work Function in Sn-Doped In2O3Films, Applied Physics Express, 3 (2010).

[43] C. Zhang, L. Qi, Q. Chen, L. Lv, Y. Ning, Y. Hu, Y. Hou, F. Teng, Plasma treatment of ITO cathode to fabricate free electron selective layer in inverted polymer solar cells, J. Mater. Chem. C, 2 (2014) 8715-8722.

[44] https://www.pveducation.org/pvcdrom/solar-cell-operation/fill-factor.

[45] D. Abou-Ras, A. Nikolaeva, S. Caicedo Dávila, M. Krause, H. Guthrey, M. Al-Jassim, M. Morawski, R. Scheer, No Evidence for Passivation Effects of Na and K at Grain Boundaries in Polycrystalline Cu(In,Ga)Se2Thin Films for Solar Cells, Solar RRL, 3 (2019).

[46] N. Nicoara, R. Manaligod, P. Jackson, D. Hariskos, W. Witte, G. Sozzi, R. Menozzi, S. Sadewasser, Direct evidence for grain boundary passivation in Cu(In,Ga)Se2 solar cells through alkali-fluoride post-deposition treatments, Nat Commun, 10 (2019) 3980.

[47] https://www.pveducation.org/pvcdrom/solar-cell-operation/open-circuit-voltage.

[48] M. Krause, A. Nikolaeva, M. Maiberg, P. Jackson, D. Hariskos, W. Witte, J.A. Marquez, S. Levcenko, T. Unold, R. Scheer, D. Abou-Ras, Microscopic origins of performance losses in highly efficient Cu(In,Ga)Se2 thin-film solar cells, Nat Commun, 11 (2020) 4189.

[49] A. Nikolaeva, M. Krause, N. Schäfer, W. Witte, D. Hariskos, T. Kodalle, C.A. Kaufmann, N. Barreau, D. Abou‐Ras, Electrostatic potential fluctuations and light‐soaking effects in Cu(In,Ga)Se2 solar cells, Prog. Photovoltaics Res. Appl., (2020).

[50] D. Abou-Ras, A. Nikolaeva, M. Krause, L. Korte, H. Stange, R. Mainz, E. Simsek Sanli, P.A. van Aken, T. Sugaya, J. Nishinaga, Optoelectronic Inactivity of Dislocations in Cu(In,Ga)Se2 Thin Films, physica status solidi (RRL) – Rapid Research Letters, (2021).

[51] R. Klenk, H.-W. Schock, Photocurrent collection in thin film solar cells-calculation and characterization for CuGaSe2/(Zn,Cd)S, in: 12th European Photovoltaic Solar Energy Conference, Amsterdam, 1994.